GiG Research Institute 95

JOURNAL OF SUSTAINABLE MINING

Volume 19 | Issue 2 Article 6

2020

Measurement of surface subsidence and ground collapse caused by underground mining in the Boleo Copper District, Mexico

TECHNICAL NOTE

Measurement of surface subsidence and ground collapse caused by underground mining in the Boleo Copper District, Mexico

Jong-Gwan Kim

Department of Energy and Resources Engineering, Chonnam National University, Republic of Korea

Abstract

Subsidence and vertical movements in mines are a challenge in mining operations. To qualify as a controlled mine site, ground movements must be measured regularly during mining operations. Boleo Copper District mine was monitored and the movement during mining operations was measured from Oct. 31, 2018 to March 15, 2019. The evaluation of vertical and horizontal movement was determined in four locations in the mine areas M303, M303S, M303 C, and M305. The exploitation area, which measured approximately 80 × 90 m^2 with a height of 2.4 m, impacted the surface in the form of cracks. These cracks were observed on the topographic surveys and varied during the mining operations from the beginning to the end. The final results indicated that the points with the greatest displacement were those in the central zone of the mine excavation (points #3, 5, and 6) and the displacement trend of the ground was toward this zone. In theory, the subsidence is typically lesser than the thickness of the extracted ore. In this case, the maximum subsidence was 1.15 m and the ore seam thickness was 2.4 m. The maximum possible subsidence is typically 55−65% of the extracted seam thickness; however, because chain pillars are generally left in place, and provide some support, this maximum possible subsidence is rarely reached. In this case, the maximum subsidence was 52% of the seam thickness.

Keywords: subsidence, vertical movements, copper mine, surface crack, long wall, underground mine

1. Introduction

When an underground ore is exploited or there are other mining-related operations such as de-watering, the stress acting within a rock mass becomes redistributed. As a result, rock mass subsidence may occur in the surface of the ground and scarps or discontinuities may be formed. The main forms of discontinuous subsidence include crown hole formation, plug subsidence, dissolution cavities, block caving, and progressive hanging wall caving. The occurrence of such subsidence may be related to the mining method involved and involve a variety of mechanisms they may also develop progressively or suddenly. During different mining stages, namely, surface and underground, subsidence occurs due to mining activities. The factors affecting or causing subsidence are revealed to be geological setting, watering, and redistribution of rock mass to ensure safety of mines [1]; and it is [1−7].

The subsidence caused during mining operations and the main forms of discontinuity include overburden formation, crown characterization, geological setting, and advanced hanging wall caving, as mentioned in the report by [1]. Many mining methods, applying different mechanisms, used in surface mining and especially in underground mining have led to subsidence during extraction or suddenly [8]. Subsidence increases due to the nature of the surrounding rocks and geological setting. Many forms of caving involve the progressive migration of an unsupported mining cavity through the overlying material to the ground's surface, and tends to form in weak overburden materials or regularly jointed rock, which progressively unravels [9, 10]. Carbonate rocks are the main cause for

Received 13 December 2019; revised 8 January 2020; accepted 9 January 2020.
Available online 5 October 2020.
E-mail address: kimjg@jnu.ac.kr.

https://doi.org/10.46873/2300-3960.1011

subsidence in mining activities. Limestone and dolomite are two models representing sudden change in water content leading to ground surface subsidence table [11, 12]; etc.) and it is [11–21]. Many accidents occur during mining activities when safety measures are absent. These accidents can partially destroy the mine site or lead to the loss of life [22, 23, 24, 25]. There are many examples of mine accidents mentioned in reports, such as the Xingtai gypsum mine in China in November 2005, gold mining in South Africa [1, 23]. Chengchao Iron Mine is an example of a large-scale production mine, which led to ground-surface collapse sinkholes observed in the eastern mine site causing dewatering. During mining exploitation and extended vertically or horizontally. Mining activities surrounding this mine were frequently subjected to the severe threat of ground movement [4, 8]. Sustainability in the mining industry is expensive (relocation, maintenance, and construction). The hole problem in the mining industry is related to the integration of the technical and operations management in addition to ensuring safe production from the mine. Several factors affect the technical constraints and production in mine stages, such as geological setting, water content, and topographical conditions around the mining site, mechanisms responsible for the collapse of the overlying strata above the mined-out areas is somewhat deficient.

This study aims to measure the collapse and evaluate the ground surface at four locations, as illustrated in Fig. 1. This technique involves observing and monitoring the surface elevation at every location. The results of investigations reveal that the collapse of the ground due to underground orebody extraction or dewatering activity in the mining area has distinctive characteristics in comparison with those seen in other underground mines (M303, M303S, M303 C, and M305).

2. Site characterization

Geotechnical characterization of the Boleo property involved evaluating the various geological structural features and depositional environments. The mineral-bearing zones of interest on the Boleo property are slightly dipping, bedded clay seams, locally called mantos, plus an overlying brecciated zone. From shallowest down, the mantos are 0, 1, 2, 3aa, 3a, 3, and 4. The manto and brecciated zones vary in thickness; however, candidate mining areas generally have a minimum thickness of at least 1.8 m. Overlying the brecciated zone is massive, relatively soft sandstone. Underlying the mantos is usually a relatively hard conglomerate with cobble;

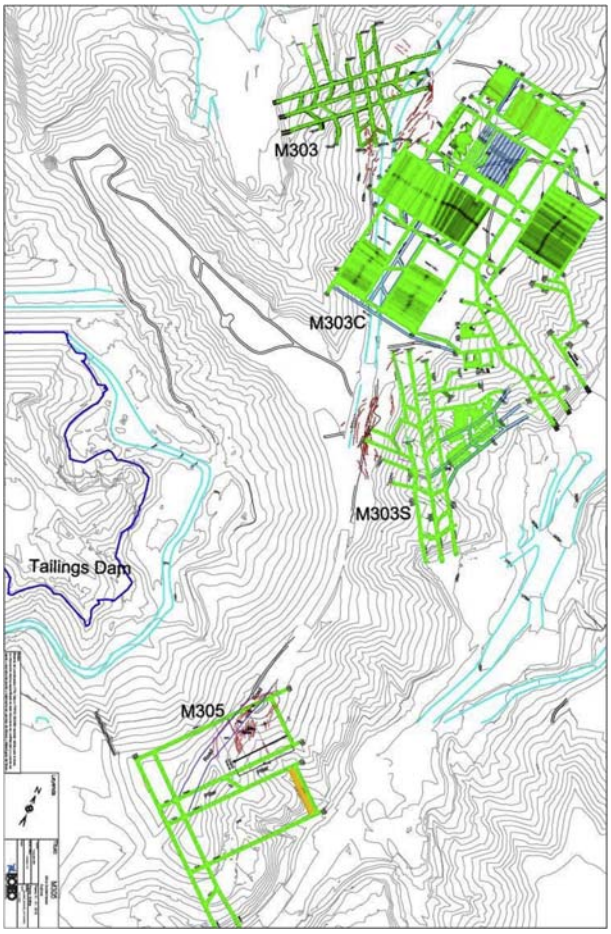

Fig. 1. Location of mines, M303, M303S, M303C, and M305.

however, in some locations, sandstone lies beneath the mantos.

This work is focused on the crack analysis of the mines located in the area known as "Mesa Soledad" of Minera Boleo. This analysis aims to determine the cause of cracks on the previous mines (M303, M303S and M303 C) and M305 that is current developing. Fig. 1 shows the location of each mine.

3. Site investigation

3.1. M303

To circumvent the Manto3 area, step mining was applied to reach the ore body after excavating through the upper interburden of Manto3. In the case of conglomerate and repeated grading to support the lateral pressure, severe abrasion and pillar damage was caused. Measurements of crack displacement and cement injection were conducted. In addition, penetration through the cracks during the rainy season was not observed, as depicted in Fig. 2.

Fig. 2. Observed cracks at M303.

3.2. M303S

After M303 mine was abandoned, three portals were developed in Soledad valley, south side. Excavation was stopped because of the inadequate effect of rock-bolt support, lack of ability to deal with the Retaque section, excessive layer separation of Manto 3A, and excessive use of wood-log support. As a result, retreat mining was executed. In the case of retreat mining, the surface cracks near the upper road of Mesa Soledad occurred; however, most of the horizontal displacement was not accompanied by severe damage, such as road destruction. Mine M303S exhibited upper cracks, as illustrated in Fig. 3.

3.3. M303 C

M303S mine site is retreat mining termination opens new portal with two entries. First application of steel arch system, various tests (shotcrete, tri-mesh, semi-shield, short wall mining, conglomerate excavation, etc.). A large number of cracks, 5–10 cm in size, were observed in the upper part of the pit area using short wall mining. Because these cracks are far from the road, they do not affect the

Fig. 3. Observed cracks at M303S.

Fig. 4. Observed cracks at M303C.

equipment or vehicles. Fig. 4 illustrates the view of cracks on site.

3.4. M305

For the purpose of short wall mining, the main gateway is excavated in the Manto3 layer and this mine has two panels. The section of panel SW1 is 80 m and 2.4 m high, and currently has advanced to approximately 90 m, which results in a volume of approximately 17,280 m^3 of extracted ore at present. This working face was started on August 6, 2018. As the production of this panel continued, some cracks were observed in the upper transportation road and valley slope. We started monitoring on October 31, 2018 in the area known as "Mesa soledad." The panel is located at an average depth of 60.68 m from the surface (Fig. 5).

4. Measurements and Monitoring

The monitoring is conducted using three main activities, namely, ground and displacement monitoring and elevation monitoring. Displacement and elevation monitoring were performed with the support of topographic surveys.

4.1. Ground and Displacement Monitoring

To investigate the ground displacement, distance-measuring points were installed, which comprised of two steel rods to measure the distance between them, perpendicular to the crack. A topographic survey of the cracks was also conducted and points on different dates were monitored to compare the location and elevation of each point with the variation of time.

Fig. 5. Observed cracks at M305.

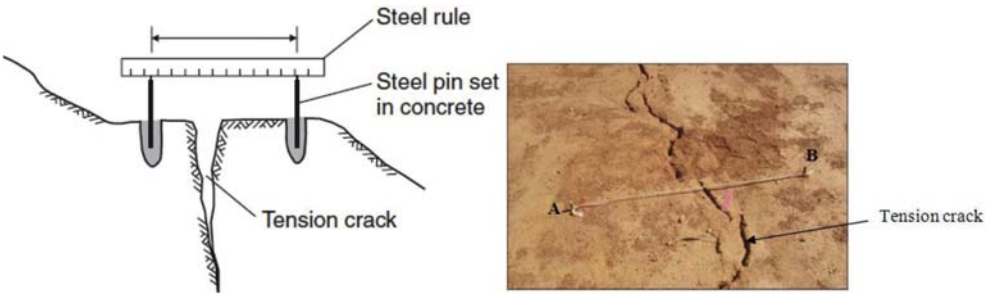

Fig. 6. Pin crack meter measuring crack displacement.

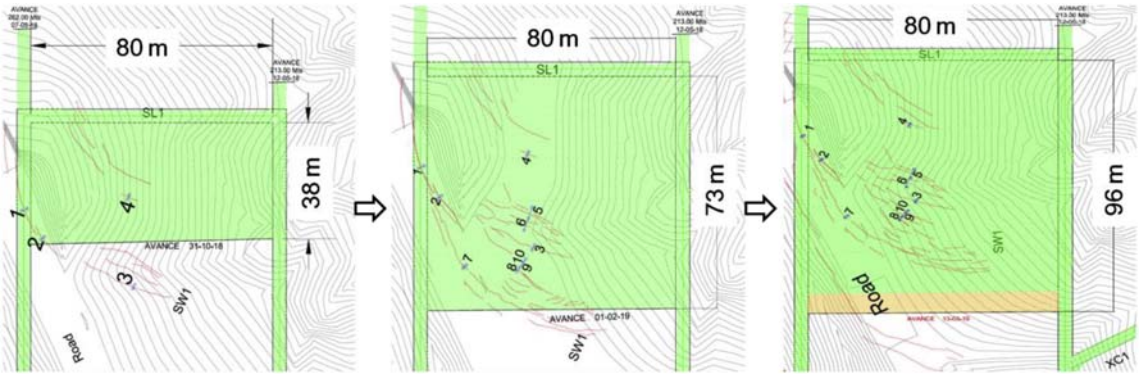

Fig. 7. Crack variation by development progress.

Measurement of width of the crack developed due tensile failure of the ground is a reliable and inexpensive means of monitoring ground movement. Fig. 6 shows the method of measuring crack widths. The simplest procedure is to install a pair of pins on either side of the crack and measure the distance between them with a steel tape.

The first four points were installed on October 31th, 2018. At that time, the total advance of the SW1 panel was 38 m. Two more points (#5 and #6) were installed in series on November 13th. Then, on December 12th points 7, 8, 9, and 10 were installed. Points 8–10 were installed in series. Point number 7 was reinstalled on January 8, 2019 due to damage caused by a car. Its new measurement was 1.332 m. Comparing the three stages, we infer that the number and length of the cracks increased significantly, as the mine production continued (Fig. 7).

The measurement of point number 7 in the last monitoring before it was damaged was 1.199 m. The second topographic survey of the cracks and points was conducted on February 1, 2019. The results of the survey established that the total advance of the SW1 panel was 73 m and the quantity of cracks considerably increased. The third survey of the cracks and the points was conducted on March 15, 2019. The result of the third topographic survey demonstrated that the points were displaced toward

Table 1. Ground monitoring results.

Point No.	31-10-2018	13-11-2018	12-12-2018	8-1-2019	15-3-2019	Total Displacement (mm)
1	1.119	1.131	1.131	1.127	1.129	10
2	1.112	1.127	1.134	1.128	1.115	3
3	1.149	1.158	1.165	1.168	1.089	−51
4	1.269	1.262	1.258	1.256	1.263	−6
5		3.693	3.622	3.604	3.487	−131
6			3.987	3.986	3.81	−153
7			1.192	1.332	1.367	42
8			1.445	1.448	1.441	−4
9			1.975	1.982	1.966	0
10			1.383	1.386	1.375	−8

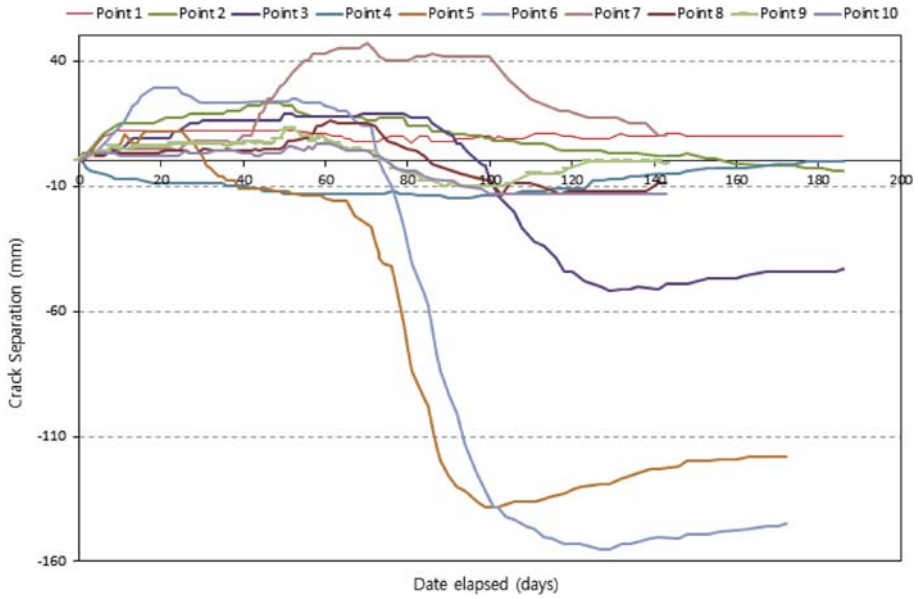

Fig. 8. Ground monitoring graph.

the center of the excavated area in SW1, which indicates towards the subsidence of the rock mass due to the excavation on M305 SW1. The three stages of the topographic survey are depicted in Fig. 7. The results of ground monitoring are presented in Table 1.

Fig. 8 depicts the total displacement with respect to the number of days passed since the installation of each point. When the third topographic survey was carried out and the points were updated on the map, it was observed that the points moved towards the central area of the mined area in M305 SW1.

4.2. Subsidence Monitoring

Table 2 lists the subsidence of each point, measured from the topographic surveys conducted on the mentioned dates. The topographic surveys were conducted by equipment capable of GPS reception (Trimble R8 GPS Receiver). The location information of the station was continuously monitored to determine the degree of subsidence, and the reference point was not set separately. The results of this table demonstrate a similar trend, as seen in Table 1. In Table 1, the measuring points #3, #5, #6 have displacements of 51, 131, and 153 mm. In Table 2, the subsidence rate of the same points are 22.7, 15.2, and 22.6 mm/day. This indicates that the highest subsidence rate is measured for points that are located in the central zone above the excavated area.

Fig. 9 depicts the subsidence status of each point; the total subsidence has a value between 40.5–1,114 mm and the maximum subsidence rate is 22.7 mm/day.

Considering a reported subsidence angle of draw of 19° as reference for similar overburden rock mass, it was calculated that the affected area is a circle

Table 2. Measurements of level and subsidence.

Point no.	Level (m)			Total subsidence (mm)	Subsidence rate (mm/day)
	1-2-2019	15-3-2019	22-3-2019		
1	263.667	263.617	263.627	40	0.8
2	263.851	263.751	263.752	98.5	2
3	262.391	261.345	261.277	1114	22.7
4	260.737	260.456	260.431	305.5	6.2
5	261.911	261.218	261.168	742.5	15.2
6	262.125	261.069	261.020	1105.5	22.6
7	264.232	264.028	264.007	224.5	4.6
8	263.201	262.407	262.327	874	17.8
9	263.030	262.166	262..082	947.5	19.3
10	262.845	261.943	261.851	993.5	20.3

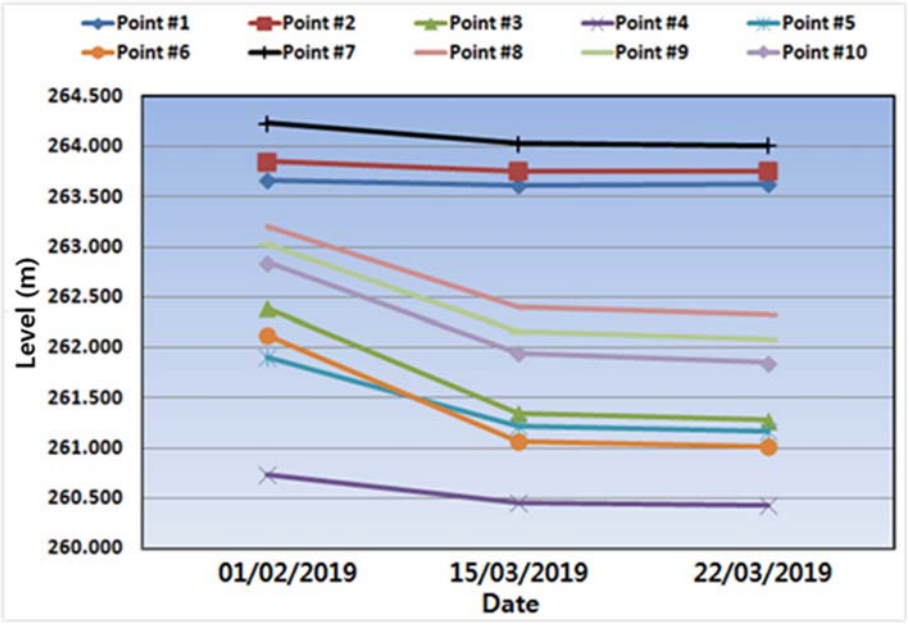

Fig. 9. Level of points plotted with respect to the number of days.

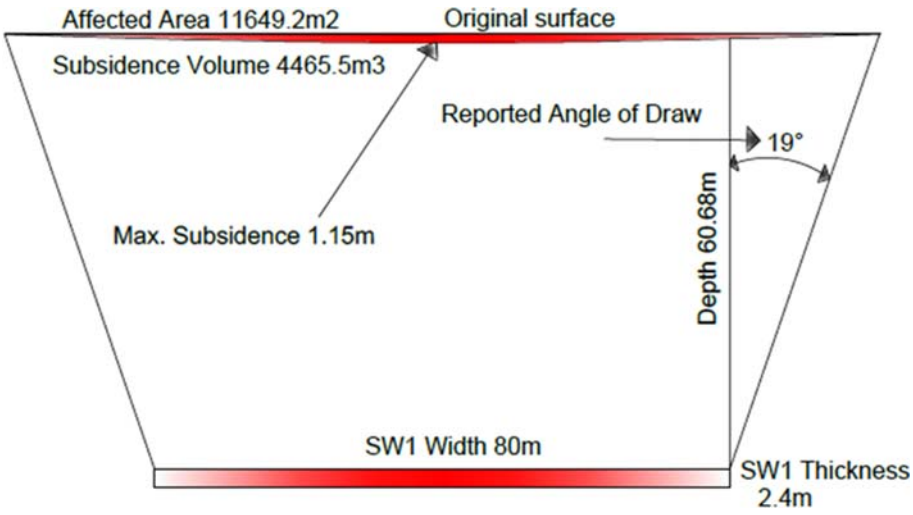

Fig. 10. True scale subsidence of M305 SW1 using a reference angle of draw.

with a diameter of 121.78 m, as SW1 is 60.68 m deep and 80 m wide, resulting in an area of 11,649.2 m^2 (see Fig. 10). Using the data obtained from the subsidence monitoring, cone geometry was assumed to calculate the subsidence volume as 4,465.5 m^3. As the ore density is 1.41 tones/m^3, the approximate subsided weight is 6,296.35 tones. By taking as reference the most remote cracks on the monitored area, it was assumed that the affected area is a 110 m diameter circle, resulting in an area of 9,503.03 m^2. As the SW1 depth is 60.68 m, the obtained angle of draw of the subsidence is 14° and the subsided volume is 3,642.9 m^3. As the ore density is 1.41 t/m^3, the approximate subsided weight is 5,136.5 tons.

5. Conclusions

The ground and displacement monitoring results indicated that the points with greater displacement were predominantly in the central zone of the mine excavation (points #3, 5, and 6) and the displacement trend of the ground pointed toward this zone. In theory, the subsidence is typically lesser than the

thickness of the extracted ore [26]. In this case, the maximum subsidence was 1.15 m and the ore seam thickness was 2.4 m. The maximum possible subsidence is typically 55–65% of the extracted seam thickness [27, 28]; however, because chain pillars are generally left in place and provide some support, the maximum possible subsidence is rarely reached. In this case, the maximum subsidence was 52% of the seam thickness. The main reason for the subsidence and cracks is the M305 underground SW1 mining. Previous cracks near M303, M303 Sur, and M303 C exhibited no effect on the cracks because they were produced directly as a result of underground mining.

The elevation monitoring results agreed with the theoretical results, indicating that the subsidence in short wall/long wall mining is higher in the central zone of the mined area and decreases as we approach the perimeter of the panel. To obtain accurate results on the rock mass subsidence volume, surveying the entire area on different occasions after the first monitoring and further comparison of the surveys is required.

Finally, this phenomenon is normally experienced when the short wall/long wall mining method is employed, which does not represent a problem inside the mine because as the working face advances, the support provided by the semishields advances along with the working face, and the goaf area is left without support, which causes the goaf to collapse resulting in subsidence on the surface ground. On the contrary, if the goaf area does not collapse immediately, this would represent a risk within the mine, as a large amount of rock mass could collapse suddenly, causing terrible damage to the personnel and the mine's machinery.

Conflicts of interest

None.

Ethical statement

Authors state that the research was conducted according to ethical standards.

Funding body

None.

Acknowledgements

My sincere gratitude for Associate professor Mahrous A. M. Ali(mahrous_mining@yahoo.co.uk, Mining and petroleum engineering dept. Faculty of Engineering, Al-Azhar University, Egypt) for his invaluable assistance to upgrade and his guidance to completed this article.

References

[1] Brady BHG, Brown ET. Rock Mechanics for Underground Mining. London: George Allen Unwin; 2006.
[2] Mancini F, Stecchi F, Gabbianelli G. GIS-based assessment of risk due to salt mining activities at Tuzla (Bosnia and Herzegovina). Eng Geol 2009;109(3–4):170–82.
[3] Vyazmensky A, Elmo D, Stead D. Role of rock mass fabric and faulting in the development of block caving induced surface subsidence. Rock Mech Rock Eng 2010;43(5):533–56.
[4] Cheng GW, Chen CX, Ma TH, Liu HY, Tang CA. A Case Study on the strata movement mechanism and surface deformation regulation in Chengchao underground iron mine. Rock Mech Rock Eng 2017;50(4):1011–32.
[5] Guarino P, Santo A, Forte G, De Falco M, Niceforo M. Analysis of a database for anthropogenic sinkhole triggering and zonation in the Naples hinterland (Southern Italy). Nat Hazards 2018;91(30):1–20.
[6] Santolo ASD, Forte G, Santo A. Analysis of sinkhole triggering mechanisms in the hinterland of Naples (Southern Italy). Eng Geol 2018;237:42–52.
[7] Xia KZ, Chen CX, Deng YY, Xiao GF, ZhengY Liu XM, Fu H, Song XG, Chen LL. In situ monitoring and analysis of the mining-induced deep ground movement in a metal mine. Int J Rock Mech Min Sci 2018;109:32–51.
[8] Huang PL. Study on Rock Movement Caused by Underground Mining in Tectonic Stress-Mines. Ph.D. thesis. Wuhan, China: Institute of Rock and Soil Mechanics, Chinese Academy of Sciences; 2008. in Chinese.
[9] Lolcama JL, Cohen HA, Tonkin MJ. Deep karst conduits, flooding, and sinkholes: lessons for the aggregates industry. Eng Geol 2002;65(2):151–7.
[10] Waltham T, Park HD, Suh J, Yu MH, Kwon HH, Bang KM. Collapses of old mines in Korea. Eng Geol 2011;118(1):29–36.
[11] Yilmaz I. GIS based susceptibility mapping of karst depression in gypsum: a case study from Sivas basin (Turkey). Eng Geol 2007;90(1):89–103.
[12] Bai H, Ma D, Chen Z. Mechanical behavior of groundwater seepage in karst collapse pillars. Eng Geol 2013;164(18):101–6.
[13] Papadopoulou-Vrynioti K, Bathrellos GD, Skilodimou HD, Kaviris G, Makropoulos K. Karst collapse susceptibility mapping considering peak ground acceleration in a rapidly growing urban area. Eng Geol 2013;158(8):77–88.
[14] Cui QL, Shen SL, Xu YS, Wu HN, Yin ZY. Mitigation of geohazards during deep excavations in karst regions with caverns: a case study. Eng Geol 2015;195:16–27.
[15] Pueyo Anchuela Ó, Casas Sainz AM, Pocoví Juan A, Gil Garbí H. Assessing karst hazards in urbanized areas. Case study and methodological considerations in the mantle karst from Zaragoza city (NE Spain). Eng Geol 2015;184(7):29–42.
[16] Duan C, Yan C, Xu B, Zhou Y. Crosshole seismic CT data field experiments and interpretation for karst caves in deep foundations. Eng Geol 2017;228:180–96.
[17] Pellicani R, Spilotro G, Gutiérrez F. Susceptibility mapping of instability related to shallow mining cavities in a built-up environment. Eng Geol 2017;217(30):81–8.
[18] Santo A, Budetta P, Forte G, Marino E, Pignalosa A. Karst collapse susceptibility assessment: a case study on the Amalfi Coast (Southern Italy). Geomorphology 2017;285:247–59.
[19] Sevil J, Gutiérrez F, Zarroca M, Desir G, Carbonel D, Guerrero J, Linares R, Roqué C, Fabregat I. Sinkhole investigation in an urban area by trenching in combination with GPR, ERT and high-precision leveling. Mantled evaporite karst of Zaragoza city, NE Spain. Eng Geol 2017;231:9–20.
[20] Gutiérrez F, Zarroca M, Linares R, Roqué C, Carbonel D, Guerrero J, McCalpin JP, Comas X, Cooper AH. Identifying the boundaries of sinkholes and subsidence areas via

trenching and establishing setback distances. Eng Geol 2018; 233:255–68.
[21] Benito-Calvo A, Gutiérrez F, Martínez-Fernández A, Carbonel D, Karampaglidis T, Desir G, Sevil J, Guerrero J, Fabregat I, García-Arnay Á. 4D monitoring of active sinkholes with a terrestrial laser scanner (TLS): a case study in the evaporite karst of the Ebro valley, NE Spain. Remote Sens 2018;10(4):571.
[22] Cooper AH, Saunders JM. Road and bridge construction across gypsum karst in England. Eng Geol 2002;65(2):217–23.
[23] Wang JA, Shang XC, Ma HT. Investigation of catastrophic ground collapse in Xingtai gypsum mines in China. Int J Rock Mech Min Sci 2008;45(8):1480–99.
[24] Villegas T, Nordlund E, Dahnér-Lindqvist C. Hangingwall surface subsidence at the Kiirunavaara mine. Sweden Eng Geol 2011;121(1–2):18–27.
[25] Fazio NL, Perrotti M, Lollino P, Parise M, Vattano M, Madonia G, Di Maggio C. A three-dimensional back-analysis of the collapse of an underground cavity in soft rocks. Eng Geol 2017;228(13):301–11.
[26] Lee FT, Abel JF. Subsidence from Underground Mining: Environmental Analysis and Planning Considerations. Geological Survey circular 1983;876:1–28.
[27] Coulthard MA, Dutton AJ. Numerical modeling of subsidence induced by underground coal mining. In: Proceedings of the 29th US Symposium: Key Questions in Rock Mechanics. Rotterdam: A.A. Balkema; 1988.
[28] Holla L. Surface subsidence prediction in the western coalfield. Mining subsidence in New South Wales, vol. 3. Sydney, Australia: Department of Minerals and Energy; 1991.